View Article Online
View Journal

Organic & Biomolecular Chemistry

Accepted Manuscript

This article can be cited before page numbers have been issued, to do this please use: J. Gong, C. Liu, S. Cai, S. He, L. Zhao and X. Zeng, *Org. Biomol. Chem.*, 2020, DOI: 10.1039/D0OB01563F.

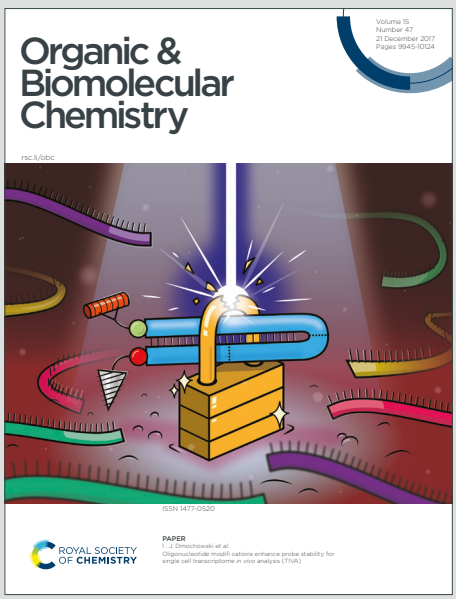

ROYAL SOCIETY OF CHEMISTRY

rsc.li/obc

View Article Online
DOI: 10.1039/D0OB01563F

ARTICLE

Novel near-infrared fluorescent probe with a large Stokes shift for sensing hypochlorous acid in mitochondria

Received 00th January 20xx,
Accepted 00th January 20xx

DOI: 10.1039/x0xx00000x

Jin Gong, [a,b] Chang Liu, [a] Songtao Cai, [a,b] Song He, [a] Liancheng Zhao [a,b] and Xianshun Zeng [a,b,*]

Hypochlorous acid (HOCl) plays a crucial role in various of physiological and pathological processes. However, it is still challenging to design a xanthene-based near-infrared (NIR) fluorescent probe with large Stokes shift for sensing HOCl. In this work, a novel mitochondria-targeted fluorescent probe **MXS** with large Stokes shift based on a xanthene-hemicyanine dyad structure has been successfully designed and synthesized for the specific detection of HOCl. Gratifyingly, the peak-to-peak Stokes shift of **MXS** was found to be 130 nm, which was obviously larger than those of conventional rhodamine dyes and most of reported xanthene-based hypochlorous acid probes. As expected, **MXS** exhibited high selectivity, high sensitivity, and fast response time (30 s) for the detection of HOCl via a specific HOCl-promoted intramolecular charge transfer processes. The detection limit of **MXS** for HOCl is calculated to be as low as 72 nM, which falls within the physiological concentration of HOCl (5–25 μM). Importantly, **MXS** is able to permeate cell membranes and accumulate in the mitochondria, which is convenient to use for monitoring the variation of hypochlorous acid concentration in the mitochondria of living cell.

Introduction

Intracellular reactive oxygen species (ROS, such as $ONOO^-$, H_2O_2, $^1O_2$, OCl^- and O_2^-) existed in living organisms played a crucial role in many physiological and pathological processes such as intracellular signal transduction, aging and immunity responses.[1] Among the various ROS, HOCl was one of the vital members, had received an increasing amount of attention due to it played as a powerful microbicidal reagent in the innate immune system.[2] However, deregulation of HOCl production and/or elimination may cause a series of organ dysfunctions and oxidative damage to nucleic acids, thereby leading to chronic inflammatory diseases, cystic fibrosis, cardiovascular disease, kidney disease, neurodegenerative disease, etc.[3] It has been reported that HOCl was generated from H_2O_2 and Cl^- by secreted myeloperoxidase (MPO) *in vivo* in response to inflammatory stimuli, and MPO were found in mitochondria of macrophage cells.[4] Therefore, the development of mitochondrial-targeted detection tools has practical significance for further understanding the distribution and functions of cellular HOCl at subcellular level and the link to the aforementioned diseases.

To date, several analytical methods have been developed for the detection of HOCl, for example, electrochemical analysis, high-performance liquid chromatography, potentiometry and colorimetry, but they are not suitable for measuring HOCl in living cells.[5] In recent years, the probe-based fluorescent imaging technology has been introduced in the detection of HOCl in the living cells due to its high sensitivity, simplicity of implementation, *in situ* analysis, spatial-temporal imaging, real-time and non-invasive detection.[6] Therefore, many efforts have recently been focused on developing efficient fluorescent probes to image HOCl by taking advantage of its strong oxidation properties.[7] Generally, these probes are composed with a fluorophore and electron-rich function moieties, and the fluorescent responses of the probe toward HOCl are based on the HOCl-promoted intramolecular charge transfer (ICT) processes.[8] Although many of HOCl-sensitive probes have been successfully utilized for the detection of HOCl in cellular environments, the probe with near-infrared (NIR) emissions and large Stokes shifts nature for real-time detection of HOCl at the subcellular level are still rare.[6h,8a,9] Especially, most of the reported rhodamine-based probes have narrow Stokes shifts (< 30 nm), which limits their intracellular imaging applications due to self-quenching and excitation wavelength interference.[10] It has been reported that the use of NIR fluorescence imaging (650-900 nm) techniques can minimize photodamage to living samples, increase tissue penetration depth, and diminish signal interference caused by autofluorescence of living samples.[11] Meanwhile, fluorescent sensors with large Stokes shifts can avoid self-quenching due to back scattering from biological samples, resulting in precise imaging and accurate sensing.[12] Consequently, the development of novel mitochondrial-targeted probes with improved emission wavelengths and Stokes shifts for understanding the functions of HOCl in

[a.] *Tianjin Key Laboratory for Photoelectric Materials and Devices, School of Materials Science & Engineering, Tianjin University of Technology, Tianjin, 300384, China. E-mail: xshzeng@tjut.edu.cn.*
[b.] *School of Materials Science and Engineering, Harbin Institute of Technology, Harbin, 150001, China.*
† Footnotes relating to the title and/or authors should appear here.
Electronic Supplementary Information (ESI) available: [details of any supplementary information available should be included here]. See DOI: 10.1039/x0xx00000x

physiological and pathological process is of considerable importance.

Bearing these concerns in mind, we herein reported a rational design and synthesis of a novel NIR mitochondria-targeted probe **MXS** with large Stokes shift for specific detection of HOCl and cell imaging at the subcellular level (**Scheme 1**). We reckoned that **MXS** with a structure of xanthene-hemicyanine dyad might increase the emission wavelengths and the Stokes shifts of the fluorophore.[13] At the same time, the incorporation of the xanthene moiety in the probe is based on the consideration of its excellent photophysical properties and biocompatibility, including high molar extinction coefficients, high quantum yields, tolerance to photobleaching, and excellent water solubility.[14] In addition, the cationic xanthene moiety normally works as a functional group for targeting mitochondria,[15] and increase the water solubility of the probe. As expected, **MXS** exhibited NIR fluorescence emission at 654 nm, large Stokes shifts (130 nm), fast response time (30 s), and high selectivity and sensitivity for the detection of HOCl via a specific HOCl-promoted intramolecular charge transfer processes. Furthermore, **MXS** is able to permeate cell membranes and highly targeted to the mitochondria and enables to be used as a probe for monitoring the variation of HOCl concentration in the mitochondria of living cells.

Results and discussion

Synthesis of MXS

The synthetic procedures for the probe **MXS** were depicted in **Scheme 1**. The key intermediate 3-diethylamino-6-methoxy-9-methylxanthine perchlorate (**E**) was synthesized starting from malonic acid and phenol *via* five steps with a moderate yield according to the literature.[16] The detailed reaction reagents and conditions were showed in **Scheme 1**. Followed by the condensation reaction of 3-diethyl-amino-6-methoxy-9-methylxanthine perchlorate (**E**) and 4-(methylthio)benzaldehyde in ethanol, the probe **MXS** was

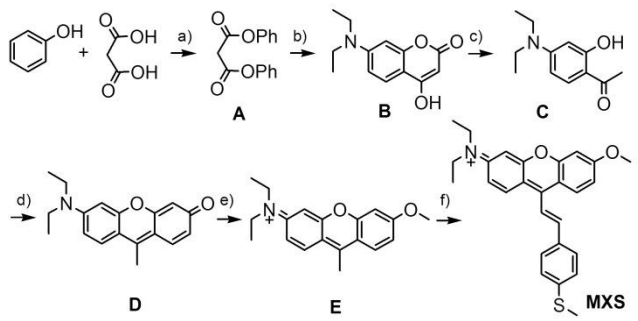

Scheme 1 Synthesis of **MXS**. Reagents and conditions: a) $POCl_3$, 0 °C to 115 °C, 1.5 h; b) 3-(diethylamino)phenol, toluene, reflux, 4 h; c) 30% H_2SO_4, 125 °C, 5 h; d) resorcinol, 85% H_3PO_4, 140 °C, 6 h; e) toluene-4-sulphonic acid methyl ester, K_2CO_3, 18-crown-6, CH_3CN, reflux, 2 h; f) 4-(methylthio)benzaldehyde, piperidine, EtOH, reflux, overnight.

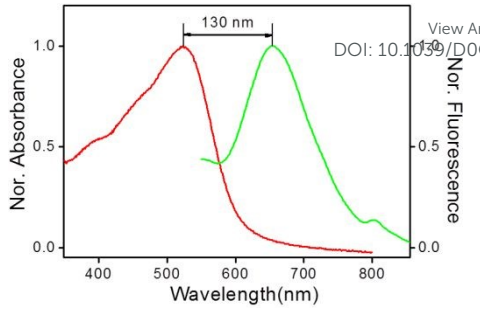

Fig. 1 Normalized absorption and fluorescence spectra of **MXS** in PBS buffer (10 mM, pH 7.4). λ_{ex} = 530 nm, slit = 10/10 nm.

obtained in 81% yield. The structure of **MXS** was fully characterized by ^{1}H NMR, ^{13}C NMR and HRMS, and the specific data were presented in the supporting information.

Optical properties of MXS

With the probe in hand, the UV/vis absorption and fluorescence emission properties, and fluorescence quantum yields of **MXS** were initially elucidated in various organic solvents (CH_3CN, DCM, DMF, DMSO, and EtOH) and in PBS buffer (10 mM, pH = 7.4). As shown in **Fig. 1**, **Table S1** and **Fig. S1**, **MXS** displayed the maxima π-π* transition absorption band at 524 nm and maxima fluorescence emission band at 654 nm (λ_{ex} = 530 nm) in PBS buffer. Comparatively, the maxima fluorescence emission band of **MXS** at 654 nm is significantly red-shifted than those of traditional rhodamine dyes (~570 nm),[17] which can be assigned to the π–π* transition of the xanthene-hemicyanine dyad fluorophore. Gratifyingly, the peak-to-peak Stokes shift of **MXS** was found to be 130 nm, which was obviously larger than those of conventional rhodamine dyes (< 30 nm).[17] At the same time, the Stokes shift of **MXS** was larger than most of reported xanthene-based hypochlorous acid probes (**Table S2**). In addition, the fluorescence quantum yields in these solvents were between 2.8% and 16.8%. Collectively, the 9-position modified **MXS** was a novel NIR fluorophore with improved Stokes shift.

Selectivity and sensing mechanism studies

In order to evaluate the recognition properties of **MXS** towards HOCl, elective experiments were carried out. The selectivity of **MXS** was scrutinized after addition of 5 equiv. oxidative species, including $^1O_2$, H_2O_2, ClO^-, NO, NO_2^-, NO_3^-, O_2^-, •OH, $ONOO^-$, and TBHP. As shown in **Fig. 2a**, upon addition of ClO^-, the intensity of the fluorescence emission of the probe at 654 nm was significantly decreased with 5 nm blue-shift. In contrast, under identical conditions, no obvious fluorescence changes in the fluorescence emission spectrum were observed after addition of 5 equiv. other oxidative species. Meanwhile, the similar decrease trend as emission spectrum was also displayed in the absorption spectrum (**Fig. S2**). Upon addition of ClO^-, the absorption intensity of the probe at 524 nm was significantly decreased. In contrast, the introduction of other oxidative species cannot lead to an obvious fluorescence change under the identical conditions. Above results showed that only ClO^- can cause the spectral change of the probe,

View Article Online
DOI: 10.1039/D0OB01563F

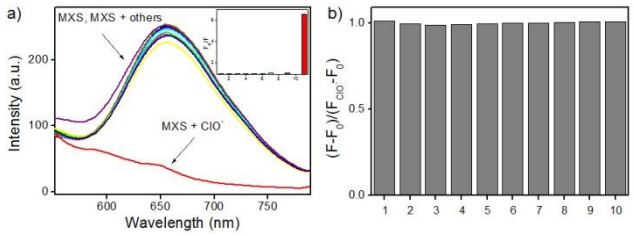

Fig. 2 a) Fluorescence responses of **MXS** (10 μM) in the presence of different relevant analytes (5 equiv.) in PBS (10 mM, pH = 7.4), 1: $^1O_2$, 2: H_2O_2, 3: blank, 4: NO, 5: NO_2^-, 6: NO_3^-, 7: O_2^-, 8: •OH, 9: $ONOO^-$, 10: TBHP, and 11: ClO^-; b) ratio $(F - F_0)/(F_{ClO} - F_0)$ of fluorescence intensity of **MXS** (10 μM) at 654 nm upon addition of 5 equiv. other analytes and 5 equiv. OCl^- in PBS, 1: ClO^-, 2: $^1O_2$, 3: H_2O_2, 4: NO, 5: NO_2^-, 6: NO_3^-, 7: O_2^-, 8: •OH, 9: $ONOO^-$, and 10: TBHP. λ_{ex} = 530 nm, slit = 10/10 nm.

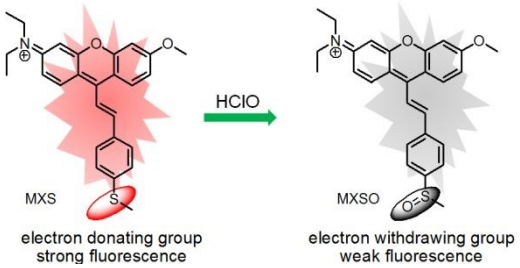

Scheme 2 The response mechanism of the probe **MXS** toward HOCl.

indicating that **MXS** showcased the high specificity for OCl^-.

According to the literatures,[8a,8c] we speculated that the spectral changes of **MXS** were initiated by HOCl-induced ICT mechanism illustrated in **Scheme 2**. After reaction with OCl^-, the electron donating sulfur atom was oxidized to yield an electron withdrawing sulfoxide, resulting in the fluorescence emission spectra and absorption spectra of the fluorophore largely decreased. To verify the speculated detection mechanism of **MXS** towards OCl^-, the high-resolution mass spectra (HRMS) was conducted to analyze the molecular weight of **MXS** after the reaction with OCl^-. As shown in **Fig. S3**, an intense peak at m/z 446.1804 corresponding to **MXSO** was distinct, providing reliable evidence for the HOCl-induced oxidation of the electron donating sulfur atom to produce the electron withdrawing sulfoxide moiety. In addition, **MXSO** was obtained by the oxidation of the sulfur group in **MXS** by using *m*-CPBA as oxidizing reagent, and the ^{1}H NMR and ^{13}C NMR spectra were presented in **Fig. S10** and **Fig. S11**. The absorption spectra, emission spectra and fluorescence quantum yields of **MXSO** were measured in various organic solvents (CH_3CN, DCM, DMF, DMSO, and EtOH) and in PBS buffer. As presented in **Table S3** and **Fig. S4**, the absorption and emission spectra of **MXSO** were consistent with those of **MXS** treated with OCl^- in PBS buffer. Furthermore, the fluorescence quantum yields in these solvents were between 1.8% and 8.2%.

To further demonstrate the specific recognition of **MXS** towards OCl^-, the competition experiments were simultaneously conducted by addition of OCl^- to the solution of **MXS** in the presence of 5 equiv. of other oxidative species ($^1O_2$, H_2O_2, NO, NO_2^-, NO_3^-, O_2^-, •OH, $ONOO^-$, and TBHP). As shown in **Fig. 2b**, in the presence of the relevant oxidative species, the probe still exhibited an obvious fluorescence change for the detection of OCl^-. These phenomena indicated that **MXS** could successfully recognize OCl^- with high selectivity over other biologically oxidative species, implying the potential for sensing OCl^- under complex physiological conditions.

Sensitivity studies

In order to further evaluate the recognition properties of **MXS** towards OCl^-, the fluorometric titration experiments were performed to investigate the sensitivity of the probe. As shown in **Fig. 3a**, upon treatment with the increasing concentrations of OCl^- (0–7 equiv.), the emissions peak of xanthene-hemicyanine dyad fluorophore at 654 nm disappeared gradually. Essentially, the fluorescence emission intensities at 654 nm became constant when the amount of OCl^- reached 5 equiv. The fluorescence intensity of **MXS** at 654 nm was linearly proportional to concentration of OCl^- within the range from 0 to 30 μM, and then data analysis reveals an excellent linear relationship with a correlation coefficient of 0.9989 (**Fig. 3b**). Subsequently, the detection limit of **MXS** towards OCl^- was calculated to be 72 nM based on the equation of 3σ/k, where k is the slope plotted from the fluorescence intensity at 654 nm versus the concentration of OCl^-, and σ is the fitting error on the intercept. Therefore, the probe can be used to detect HOCl down to 72 nM, which falls within the physiological concentration of HOCl (5–25 μM).[18] Hence, we can apply this probe effectively for biological applications. Compared with other xanthene-based fluorescent probes for detecting OCl^-, the detection limit of **MXS** was at a relatively low level (**Table S2**). Meanwhile, after the addition of OCl^- (0–7 equiv.) to the solution, the absorption intensity of **MXS** at 524 nm remarkably decreased and reached the plateau when the

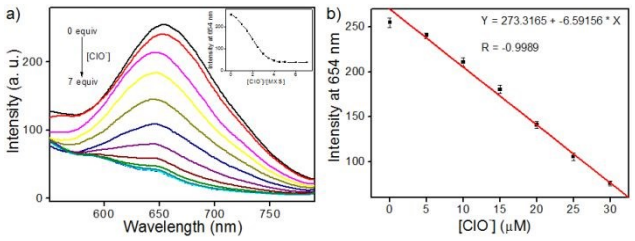

Fig. 3 a) The fluorescence changes of **MXS** (10 μM) treated with increasing concentrations of OCl^- (0 – 7 equiv.). Insert: The plot of the fluorescence intensities at 654 nm versus the equivalents of OCl^-; b) The plot of the fluorescence intensities of **MXS** at 654 nm versus the concentrations of OCl^- (0 – 30 μM). The conditions: PBS buffer (10 mM, pH 7.4), λ_{ex} = 530 nm, slit = 10/10 nm.

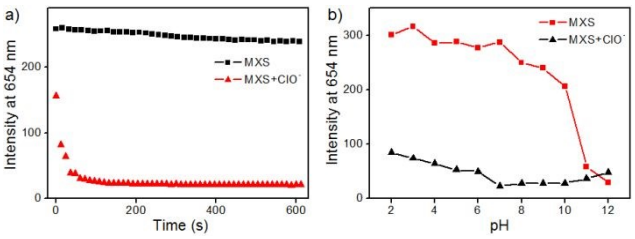

Fig. 4 a) Time-dependent fluorescence response of **MXS** (10 μM) in the absence/presence of OCl^- (5 μM); b) Fluorescence intensity at 654 nm of **MXS** (10 μM) at different pH values in the absence/presence of OCl^- (5 μM). The conditions: PBS buffer (10 mM, pH 7.4), λ_{ex} = 530 nm, slit = 10/10 nm.

accumulated amount of OCl^- reached 5 equiv. (**Fig. S5**). These results indicated that **MXS** showed high sensitivity to OCl^- and could be used as a practical probe for quantitative detection OCl^- in aqueous environments.

Time- and pH-dependent fluorescent responses of MXS

Subsequently, in order to assess the possibility of **MXS** for sensing OCl^- in real-time, time-dependent fluorescent responses of **MXS** towards OCl^- were evaluated at room temperature. As shown in **Fig. 4a**, in the presence of 5 equiv. of OCl^-, the fluorescence intensity of **MXS** at 654 nm rapidly decreased and reached a plateau within about 30 s, suggesting that **MXS** could be used as an effective candidate for monitoring OCl^- in real-time. In contrast, in the absence of OCl^-, the probe showed almost stable emission signals output when continuously excited under a 530 nm laser within 600 s, indicating that **MXS** could be stably present in the solution and owned high photo-stability. In addition, due to the differences in the pH values in various cell ompartments,[19] keeping the stable output of the fluorescence signal in acidic, neutral and alkaline environments is a very important property of the probe. Therefore, the fluorescent response of **MXS** towards OCl^- at different pH conditions (ranging from 2.0 to 12.0) were further assessed to explore the optimal working range of the probe and to apply **MXS** in complicated systems, especially biological systems. As shown in **Fig. 4b,** the fluorescence intensity of **MXS** at 654 nm was stable in the pH range from 2.0 to 10.0. In contrast, upon addition of OCl^-, the fluorescence signals of the probe **MXS** decreased dramatically in the pH range of 2.0–10.0. The broad pH tolerance for the detection of OCl^- and the stable fluorescence of the probe at a pH level of approximately 7.4 suggested that **MXS** had the possibility to detect OCl^- in biological systems.

Application of MXS in living cells

Inspired by the excellent spectral properties of **MXS**, such as high selectivity, high sensitivity, response in real time, and physiological pH range of working, potential applications of the probe for imaging Cys in living cells were investigated next. As standard MTT assays confirmed that **MXS** has fairly low toxicity towards living cells when the concentration of the probe was 0–20 μM and the cells were incubated for 24 h (**Fig. S6**), we evaluated whether **MXS** can image HOCl in living cells by means of laser scanning confocal microscopy. HeLa cells were incubated with **MXS** for 30 min in the growth medium, and then washed three times with PBS to remove excess probes. As presented in **Fig. 5a**, strong emission signals in the red channel were observed with an excitation of 559 nm in the cells. In contrast, after treatment with OCl^- (5 μM) and then fed for another 30 min, the fluorescence outputs in 618–718 nm were largely decreased (**Fig. 5b**). Compared with the untreated cells, the relative decrease of fluorescence signals is about 3-fold (**Fig. 5c**). Thus, above-described results revealed that **MXS** had good membrane permeability and could be used for imaging OCl^- in living cells.

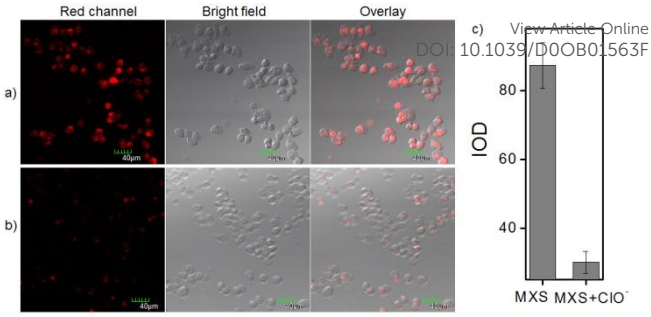

Fig. 5 Fluorescence images of HeLa cells. a) Cells were incubated with **MXS** (1 μM) for 30 min; b) and then incubated with OCl^- (5 μM) for 30 min; c) Histogram of fluorescence enhancement. λ_{ex} = 559 nm, λ_{em} = 618 – 718 nm.

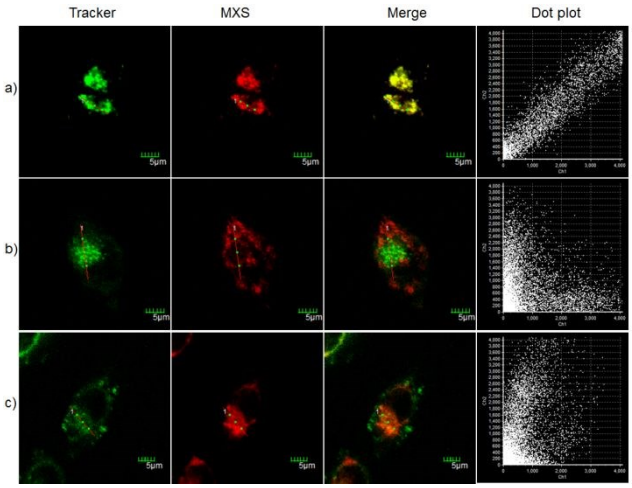

Fig. 6 Fluorescence imaging of HeLa cells costained with **MXS** (1 μM) upon treatment of and Mito-Tracker Green (200 nM), Lyso-Tracker Green Green (200 nM), or ER-Tracker Green (200 nM). Cells were incubated with probes at 37 °C for 30 min, and then treated with OCl^- (5 μM) for another 30 min, and washed before imaging. a) Costained with Mito-Tracker Green; b) Costained with Lyso-Tracker Green, c) Costained with ER-Tracker Green; Red channel: λ_{ex} = 559 nm, λ_{em} = 607-683 nm. Green channel: λ_{ex} = 488 nm, λ_{em} = 509-544 nm.

Comparing the fluorescence images with the bright field images, non-uniform intracellular fluorescence signals of **MXS** were noticed in **Fig. 5**, implying that the probe were located in some specific organelles. In order to verify our speculation, the cellular distribution properties of **MXS** were explored by colocalization with the commercial subcellular organelle reagents, namely, Lyso-Tracker Green (Lyso), Mito-Tracker Green (Mito), and ER-Tracker Green (ER), respectively. In addition, due to the cationic and lipophilic characters of many xanthene dyes, such as tetramethylrhodamine and rhodamine 123, they were widely used as mitochondrial tracers in living cells.[15] As presented in **Fig. 6a**, the fluorescence signal of **MXS** overlapped perfectly with that of Mito, indicating that **MXS** was predominantly accumulated in the mitochondria. Meanwhile, the intensity scatter plot of the red channel and the green channel showed a high correlation between **MXS** and Mito with high Pearson's coefficient (0.97) and overlap coefficient (0.97), respectively. In contrast, the low overlap coefficients and Pearson's coefficients of **MXS** and other organelle tracers (Lyso, and ER) implied that they were located in different regions (**Fig.**

View Article Online
DOI: 10.1039/D0OB01575F

6b–c). Thus, the results of the co-localization experiments indicated that **MXS** can precisely target the mitochondria and can be employed for imaging of HOCl in the mitochondria of living cells.

Conclusions

In summary, a novel mitochondria-targeted fluorescent probe **MXS** with large Stokes shift based on a xanthene-hemicyanine dyad structure has been successfully designed and synthesized for the specific detection of HOCl. As expected, **MXS** exhibited NIR fluorescence emission at 654 nm, large Stokes shifts of 130 nm, fast response time (30 s), and high selectivity and sensitivity for the detection of HOCl *via* a specific HOCl-promoted intramolecular charge transfer processes. Importantly, **MXS** is able to permeate cell membranes and accumulate in the mitochondria, which is convenient to use for monitoring the variation of HOCl concentration in the mitochondria of living cell.

Experimental

Materials and instruments

All reagents used in the experiments were purchased from J&K Scientific Ltd, and were used directly unless otherwise stated. The water used in the experiments was double distilled water. The progress of the reaction was monitored by observing a thin layer chromatography under an ultraviolet lamp. Absorption spectra and fluorescence emission spectra were measured on UV-2550 UV/Vis spectrophotometer (Hitachi Japan) and F-4600 fluorescence spectrophotometer (Hitachi Japan), respectively. All fluorescence spectra data were tested at an excitation wavelength of 530 nm with an excitation/emission slit width of 10/10 nm. ^{1}H NMR (400 MHz) and ^{13}C NMR (100 MHz) spectra were collected by Bruker spectrometer. Chemical shift (δ) values are in ppm and tetramethylsilane is used as an internal standard. High resolution mass spectra (HRMS) were measured by Agilent 6510 Q-TOF LC/MS instrument (Agilent Technologies, Palo Alto, CA) equipped with an electrospray ionization (ESI) source. The pH was measured using a FE 20/EL 20PH meter (Mettler-Toledo Instruments (Shanghai) CO., Ltd.). Cell imaging was conducted by Olympus FV 1000-IX81 laser scanning confocal imaging.

Synthesis of MXS

After dissolving 3-diethylamino-6-methoxy-9-methylxanthylium perchlorate (395 mg, 1 mmol) and 4-(methylthio)benzaldehyde (152 mg, 1 mmol) in absolute ethanol (10 mL), a drop of piperidine was added, and then the reaction system was refluxed overnight. After cooling, it was evaporated to dryness under vacuum, and then the crude product was purified by silica gel column to afford the compound **MXS** as a red solid (104 mg, 23% yield). M.p. 84 – 86 °C; ^{1}H NMR (400 MHz, $CDCl_3$) δ 8.19 (d, *J* = 9.7 Hz, 1H), 8.12 (d, *J* = 9.8 Hz, 1H), 7.80 – 7.71 (m, 1H), 7.67 (d, *J* = 8.3 Hz, 2H), 7.33 – 7.31 (m, 2H), 7.23 (d, *J* = 8.0 Hz, 2H), 7.15 – 7.13 (m, 2H), 6.92 (s, 1H), 4.02 (s, 3H), 3.70 (dd, *J* = 14.1, 6.9 Hz, 4H), 2.50 (s, 3H), 1.36 (t, *J* = 7.0 Hz, 6H); ^{13}C NMR (100 MHz, $CDCl_3$) δ 167.30, 158.61, 157.11, 155.47, 146.98, 143.57, 132.12, 131.39, 129.83, 129.31, 128.96, 126.61, 125.94, 117.25, 116.98, 116.60, 114.91, 114.17, 100.68, 96.68, 56.77, 46.68, 31.94, 29.71, 14.99; HRMS m/z = 430.1841 calcd for $C_{29}H_{28}NO_4^+$ $[M]^+$, found: 430.1847.

Cell culture and fluorescence imaging

HeLa cells were cultured in DMEM medium supplemented with 10% (v/v) fetal bovine serum (FBS) and penicillin/streptomycin (100 μg/mL) in an atmosphere of 5% CO_2 at 37 °C. Then, HeLa cells were seeded in a 96-well plate, and cultured in an incubator for 2 hours to adhere to the plate, and then subjected to cell imaging experiments. The cells were incubated with **MXS** (1 μM) for 30 minutes, and then NaOCl (5 μM) was added and incubated for another 30 minutes. For co-localization experiments, **MXS** (1 μM) were incubated with a 200 nM trackers (Mito-Tracker Green (Mito), ER-Tracker Green (ER), and Lyso-Tracker Green (Lyso)) for 30 minutes, respectively, and then treated with NaOCl (5 μM) for another 30 min. Prior to cell imaging, the medium was washed three times with PBS buffer to remove excess probes and trackers.

MTT assay

The HeLa cells were cultured for 12 hours, and then **MXS** at a concentration of 0, 1, 3, 5, 10, 20 μM were separately added to per well and were again incubated for 24 hours. The treated cells were added to 0.012 M of 3-(4,5-dimethylthiazol-2-yl)-2,5-diphenyltetrazolium bromide solution per well, and then incubated again 4 hours. The medium was aspirated and then placed in 100 μL DMSO for another two hours, and the absorbance at 490 nm was measured.

Conflicts of interest

There are no conflicts to declare.

Acknowledgements

This work was sponsored by the National Natural Science Foundation of China (NNSFC 21907075; 21272172), and the Natural Science Foundation of Tianjin City (19JCZDJC32400; 18JCQNJC75900).

Notes and references

1 (*a*) S. G. Rhee, *Science*, 2006, **312**, 1882; (*b*) Y. Cui, Z. Lu, L. Bai, Z. Shi, W. Zhao and B. L. Zhao, *Eur. J. Cancer*, 2007, **43**, 2590; (*c*) Y. Tang, F. Feng, F. He, S. Wang, Y. Li and D. Zhu, *J. Am. Chem. Soc.*, 2006, **128**, 14972; (*d*) M. Schieber and N. S. Chandel, *Curr. Biol.*, 2014, **24**, 453.
2 (*a*) A. Daugherty, J. L. Dunn, D. L. Rateri and J. W. Heinecke, *J. Clin. Invest.*, 1994, **94**, 437; (*b*) S. M. Wu and S. V. Pizzo, *Arch. Biochem. Biophys.,* 2001, **391**, 119; (c) K. C. Huang, C. C. Yang, K. T. Lee and C. T. Chien, *Kidney Int.*, 2003, **64**, 704.
3 (*a*) H. Zhu, J. Fan, J. Wang, H. Mu and X. Peng, *J. Am. Chem. Soc.*, 2015, **136**, 12820; (*b*) D. Pattison and M. Davies, *Chem. Res. Toxicol.*, 2001, **14**, 1453. (*c*) Y. W. Yap, M. Whiteman and

N. S. Cheung, *Cell Signal,* 2007, **19**, 219; (*d*) M. J. Steinbeck, L. J. Nesti, P. F. Sharkey and J Parvizi,. *J. Orthop. Res*., 2007, **25**, 1128.

4 (*a*) C. C. Winterbourn, M. B. Hampton, J. H. Livesey and A. J. Kettle, *J. Biol. Chem*., 2006, **281**, 39860; (*b*) D. I. Pattison and M. J. Davies, *Chem. Res*. *Toxicol*., 2001, **14**, 1453; (*c*) A. J. Kettle and C. C. Winterbourn, *Redox Rep*., 1997, **3**, 3.

5 L. Moberg and B. Karlberg, *Anal. Chim. Acta,* 2000, **407**, 127.

6 (*a*) M. Sun, H. Yu, H. Zhu, F. Ma, S. Zhang, D. Huang and S. Wang, *Anal. Chem*., 2014, **86**, 671; (*b*) J. J. Hu, N.-K. Wong, M.-Y. Lu, X. Chen, S. Ye, A. Q. Zhao, P. Gao, R. Y.-T. Kao, J. Shen and D. Yang, *Chem. Sci.*, 2016, **7**, 2094; (*c*) H. Ma, B. Song, Y. Wang, D. Cong, Y. Jiang and J. Yuan, *Chem. Sci*., 2017, **8**, 150; (*d*) P. Wei, W. Yuan, F. Xue, W. Zhou, R. Li, D. Zhang and T. Yi, *Chem. Sci*., 2018, **9**, 495; (*e*) Y. Tang, D. Lee, J. Wang, G. Li, J. Yu, W. Lin and J. Yoon, *Chem. Soc. Rev*., 2015, **44**, 5003; (*f*) S. Kenmoku, Y. Urano, H. Kojima and T. Nagano, *J. Am. Chem. Soc*., 2007, **129**, 7313; (g) X. Jiao, C. Liu, Q. Wang, K. Huang, S. He, L. Zhao and X. Zeng, *Anal. Chim. Acta*, 2017, **969**, 49; (*h*) C. Liu, Q. Wang, X. Jiao, H. Yao, S. He, L. Zhao and X. Zeng, *Dyes Pigm.,* 2019, **160**, 989; (i) K. Huang, S. He and X. Zeng, *Tetrahedron Lett.*, 2017, **58**, 2004; (j) L. Liang, C. Liu, X. Jiao, L. Zhao and X. Zeng, *Chem. Commun.,* 2016, **52**, 7982.

7 (*a*) J. J. Hu, N.-K. Wong, Q. Gu, X. Bai, S. Ye and D. Yang, *Org. Lett.,* 2014, **16**, 3544; (*b*) J. J. Hu, N.-K. Wong, M.-Y. Lu, X. Chen, S. Ye, A. Q. Zhao, P. Gao, R. Yi-Tsun Kao, J. Shen and D. Yang, *Chem. Sci.,* 2016, **7**, 2094; (*c*) G. Cheng, J. Fan, W. Sun, J. Cao, C. Hu and X. Peng, *Chem. Commun.*, 2014, **50,** 1018; (*d*) L. Wu, I. C. Wu, C. C. DuFort, M. A. Carlson, X. Wu, L. Chen, C.-T. Kuo, Y. Qin, J. Yu, S. R. Hingorani and D. T. Chiu, *J. Am. Chem. Soc.*, 2017, **139**, 6911; (*e*) Q. Xu, C. H. Heo, G. Kim, H. W. Lee, H. M. Kim and J. Yoon, *Angew. Chem., Int. Ed*., 2015, **54**, 4890; (*f*) W. Zhang, W. Liu, P. Li, J. kang, J. Wang, H. Wang and B. Tang, *Chem. Commun*., 2015, **51**, 10150.

8 (*a*) X. Jiao, K. Huang, S. He, C. Liu, L. Zhao and Xianshun Zeng, *Org. Biomol. Chem*., 2019, **17**, 108; (*b*) H. Xiao, K. Xin, H. Dou, G. Yin, Y. Quan and R. Wang, *Chem. Commun*., 2015, **51**, 1442; (*c*) Z. R. Grabowski, K. Rotkiewicz and W. Rettig, *Chem. Rev.*, 2003, **103**, 3899; (*c*) M. Vedamalai, D. Kedaria, R. Vasita and I. Gupta, *Sens. Actuators, B,* 2018, **263**, 137; (d) C. Liu, X. Jiao, S. He, L. Zhao and X. Zeng, *Talanta* 2017, **174**, 234.

9 (*a*) Y. Yue, F. Huo, C. Yin, J. Escobedo and R. M. Strongin, *Analyst*, 2016, **141**, 1859; (*b*) X. Chen, F. Wang, J. Hyun, T. Wei, J. Qiang, X. Ren, I. Shin and J. Yoon, *Chem. Soc. Rev*., 2016, **45**, 2976.

10 (*a*) Z. Zhang and S. Achilefu, *Org. Lett.,* 2004, **6**, 2067; (*b*) J. M. Baumes, J. J. Gassensmith, J. Giblin, J. J. Lee, A. G. White, W. J. Culligan, W. M. Leevy, M. Kuno and B. D. Smith, *Nat. Chem.,* 2010, **2**, 1025; (*c*) X. Wang, L. Cui, N. Zhou, W. Zhu, R. Wang, X. Qian and Y. Xu, *Chem. Sci.,* 2013, **4**, 2936; (*d*) F. Wei, Y. Lu, S. He, L. Zhao and X. Zeng, *Anal. Methods*, 2012, **4**, 616; (*e*) F. Wei, Y. Lu, S. He, L. Zhao and X. Zeng, *J. Fluoresc.*, 2012, **22**, 1257; (f) D. Zheng, X. Qiu, C. Liu, X. Jiao, S. He, L. Zhao and X. Zeng, *New J. Chem.*, 2018, **42**, 5135.

11 (*a*) Z. Q. Guo, S. Park, J. Yoon and I. Shin, *Chem. Soc. Rev.,* 2014, **43**, 16; (*b*) R. Weissleder and V. Ntziachristos, *Nat. Med.,* 2003, **9**, 123; (*c*) A. N. Butkevich, G. Lukinavičius, E. D'Este and S. W. Hell, *J. Am. Chem. Soc.,* 2017, **139**, 12378; (*d*) L. Yuan, W. Lin, K. Zheng, L. He and W. Huang, *Chem. Soc. Rev.,* 2013, **42**, 622; (*e*) C. Liu, X. Jiao, Q. Wang, K. Huang, S. He, L. Zhao and X. Zeng, *Chem. Commun.*, 2017, **53**, 10727; (*f*) Q. Wang, K. Huang, S. Cai, C. Liu, X. Jiao, S. He, L. Zhao and X. Zeng, *Org. Biomol. Chem.*, 2018, **16**, 7609; (g) S. Cai, C. Liu, X. Jiao, S. He, L. Zhao and X. Zeng, *Org. Biomol. Chem.*, 2020, **18**, 1148; (h) S. Cai, C. Liu, X. Jiao, L. Zhao and X. Zeng, *J. Mater. Chem. B*, 2020, **8**, 2269; (i) J. Gong, C. Liu, X. Jiao, S. He, L. Zhao and X. Zeng, *J. Mater. Chem. B*, 2020, **8**, 2343.

12 T. Ren, W. Xu, W. Zhang, X. Zhang, Z. Wang, Z. Xiang, L. Yuan and X. Zhang, *J. Am. Chem. Soc.,* 2018, **140**, 7716.

13 (*a*) Y. Li, S. He, Y. Lu and X. Zeng, *Org. Biomol. Chem*. 2011, **9**, 2606; (*b*) Y. Li, S. He, Y. Lu, L. Zhao and X. Zeng, *Dyes Pigment*, 2013, **96**, 424.

14 (*a*) M. Beija, C. A. M. Afonso and J. M. G. Martinho, *Chem. Soc. Rev.,* 2009, **38**, 2410; (*b*) D. T. Quang and J. S. Kim, *Chem. Rev.,* 2010, **110**, 6280; (*c*) Y. Yang, Q. Zhao, W. Feng and F. Li, *Chem. Rev.*, 2012, **113**, 192; (*d*) K. P. Carter, A. M. Young and A. E. Palmer, *Chem. Rev.*, 2014, **114**, 4564.

15 Y. K. Kim, H. H. Ha, J. S. Lee, X. Bi, Y. H. Ahn, S. Hajar, J. J. Lee and Y. T. Chang, *J. Am. Chem. Soc.,* 2010, **132**, 576.

16 (*a*) J. Liu, Y. Q. Sun, Y. Huo, H. Zhang, L. Wang, P. Zhang, D. Song, Y. Shi and W. Guo, *J. Am. Chem. Soc.*, 2014, **136**, 574; (*b*) Y. M. Poronik, M. P. Shandura and Y. Kovtun, *Dyes Pigment*., 2007, **72**, 199.

17 M. Beija, C. A. M. Afonso and J. M. G. Martinho, *Chem. Soc. Rev.,* 2009, **38**, 2410.

18 (*a*) M. Katrantzis, M. S. Baker, C. J. Handley and D. A. Lowther, *Free Radical Biol. Med*., 1991, **10**, 101; (*b*) M. R. McCall, A. C. Carr, T. M. Forte and B. Frei, *Arterioscler. Thromb. Vasc. Biol*., 2001, **21**, 1040.

19 O. A. Krasheninina, D. S. Novopashina, A. A. Lomzov and A. G. Venyaminova, *Chem. Bio. Chem*., 2014, **15**, 1939.

View Article Online
DOI: 10.1039/D0OB01563F

Novel near-infrared fluorescent probe with a large Stokes shift for sensing hypochlorous acid in mitochondria

Jin Gong, Chang Liu, Songtao Cai, Song He, Liancheng Zhao and Xianshun Zeng

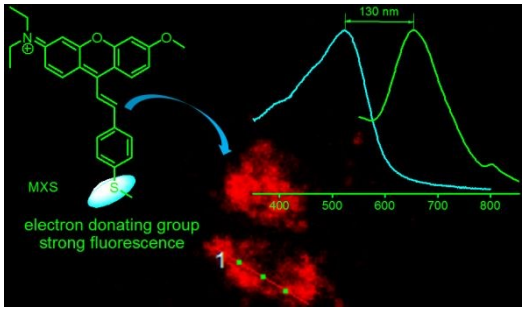

A novel mitochondria-targeted fluorescent probe **MXS** with large Stokes shift (130 nm) based on a xanthene-hemicyanine dyad structure has been successfully designed and synthesized for the specific detection of HOCl.

View Article Online
DOI: 10.1039/D0OB01563F

Novel near-infrared fluorescent probe with a large Stokes shift for sensing hypochlorous acid in mitochondria

Jin Gong [†, ‡], Chang Liu [†], Songtao Cai [†, ‡], Song He [†], Liancheng Zhao [†, ‡], Xianshun Zeng [*, †, ‡]

[†] Tianjin Key Laboratory for Photoelectric Materials and Devices, School of Materials Science & Engineering, Tianjin University of Technology, Tianjin, 300384, China

[‡] School of Materials Science and Engineering, Harbin Institute of Technology, Harbin, 150001, China

*E-mail: xshzeng@tjut.edu.cn

Contents

View Article Online
DOI: 10.1039/D0OB01563F

Synthesis of MXSO:

Upon addition of the *m*-CPBA (1 mmol, 172 mg) to compound **MXS** (1 mmol, 430 mg) in dry dichloromethane under ice bath, the temperature was naturally raised to room temperature, and the reaction was carried out for 8 hours under vigorous stirring. After removing the solvent under vacuum, the crude product was purified by silica gel column to afford a pure red solid product **MXSO** (272 mg, 61 % yield). HRMS m/z = 446.1790 calcd for $C_{27}H_{28}NO_3S^+$ $[M]^+$, found: 446.1796. ^{1}H NMR (400 MHz, $CDCl_3$) δ 8.17 (d, *J* = 8.6 Hz, 1H), 8.11 (d, *J* = 8.8 Hz, 1H), 7.94 (d, *J* = 8.1 Hz, 2H), 7.84 (d, *J* = 16.3 Hz, 1H), 7.72 (d, *J* = 8.0 Hz, 2H), 7.30-7.28 (m, 2H), 7.17-7.14 (m, 2H), 6.85 (s, 1H), 4.01 (s, 3H), 3.71 (s, 4H), 2.88 (s, 3H), 1.37 (s, 6H). ^{13}C NMR (100 MHz, $CDCl_3$) δ 167.70, 158.88, 158.64, 158.23, 157.47, 156.56, 154.97, 144.24, 144.07, 138.33, 132.22, 130.00, 129.38, 124.81, 121.17, 117.35, 116.89, 116.22, 115.41, 114.21, 113.38, 100.64, 96.65, 56.76, 46.78, 42.47, 30.92, 29.69, 27.93.

Table S1 Spectral data of **MXS** in different solvents.

Solvents	λ_{abs} (nm)	λ_{em} (nm)	ε (mol^{-1}cm^{-1}L)	Φ^a
DCM	532	662	26000	0.168
EtOH	530	661	19000	0.113
DMSO	538	674	20000	0.064
PBS	524	654	20100	0.028
MeCN	528	669	23600	0.054
DMF	533	664	8900	0.085

^{a} Relative fluorescence quantum yield estimated by using Nile Blue (Φ_B = 0.27 in ethanol)[1] as a fluorescence standard.

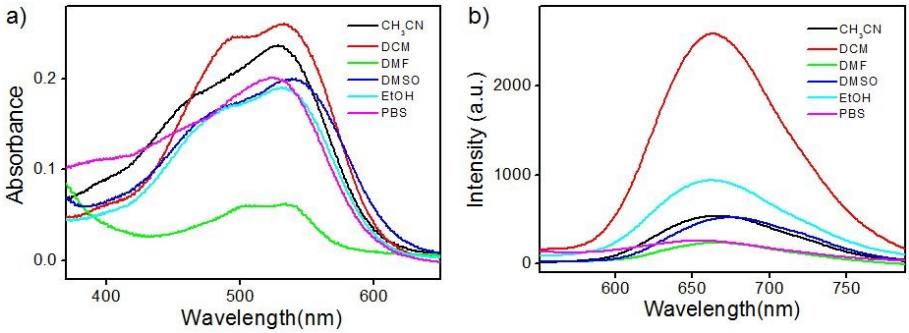

Fig. S1. Absorption and fluorescence spectra of **MXS** in different solvents.

View Article Online
DOI: 10.1039/D0OB01563F

Table S2. Comparison of **MXS** with reported probes.

Structure	Stokes shifts (nm)	Emission (nm)	LOD (nM)	Reference
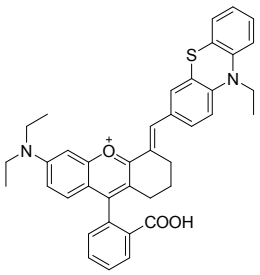	97	672	92	*Org. Biomol. Chem., 2019, 17, 108–114*
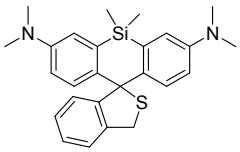	18	670	-	*J. Am. Chem. Soc. 2011, 133, 5680–5682*
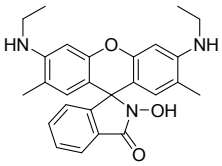	17	547	25	*Org. Lett., 2009, 859-861,*
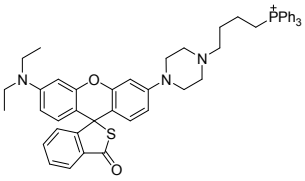	27	580	9	*Chem. Sci., 2015, 6, 4884-4888*
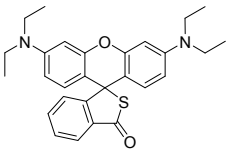	18	579	300	*Sensors and Actuators B, 2010, 150, 774–780*
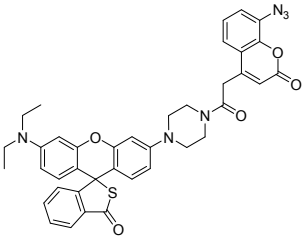	35	580	192.1	Anal. Chem. 2018, 90, 7510-7516
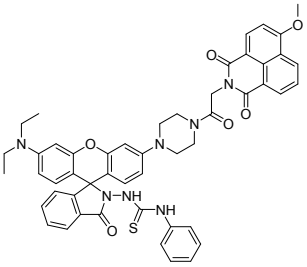	50	618	4.5	Tetrahedron, 2020, 76, 131291

View Article Online
DOI: 10.1039/D0OB01563F

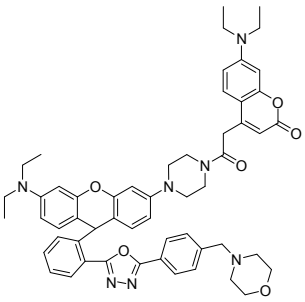	12	582	12	*Spectrochimica Acta Part A: Molecular and Biomolecular Spectroscopy, 2019, 223, 117355*
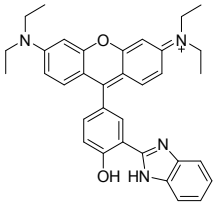	18	581	52	*Sensors and Actuators B: Chemical, 2020,304, 127299*
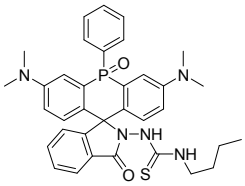	20	730	10	*Sensors & Actuators: B. Chemical, 2020, 307, 127652*
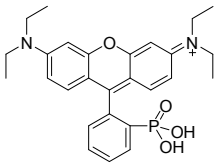	20	570	52	*Sensors & Actuators: B. Chemical, 2019, 291, 207–215*
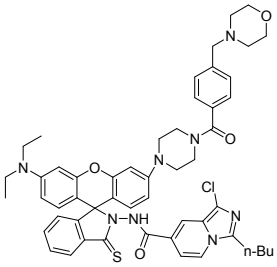	19	589	10.2	*Analytica Chimica Acta, 2019, 1052, 124-130*
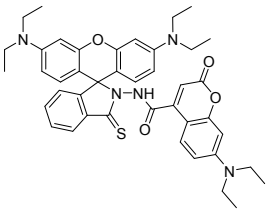	22	590	140	*Spectrochimica Acta Part A: Molecular and Biomolecular Spectroscopy, 2019, 219, 232–239*
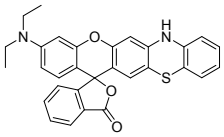	97	730	2.3	*Dyes and Pigments, 2019, 160, 989–994*
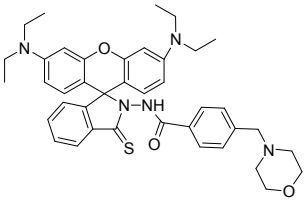	24	592	71.5	*Analytica Chimica Acta, 2019, 1046, 185-191*

View Article Online
DOI: 10.1039/D0OB01563F

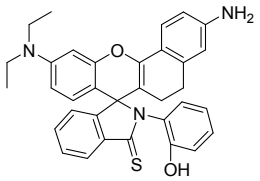	40	630	40	*Talanta, 2019, 192, 128–134*
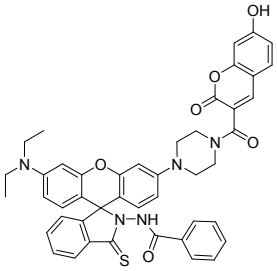	20	585	42	*Talanta, 2018, 186, 65–72*
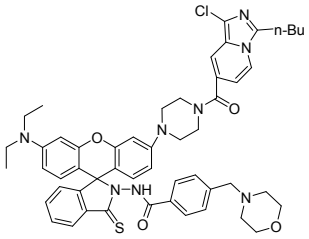	23	588	27	*Sensors and Actuators B, 2018, 263, 252–257*
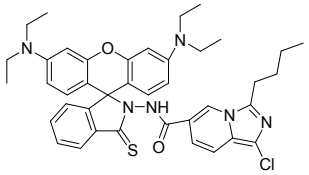	19	587	2080	*Dyes and Pigments, 2018, 148, 206-211*
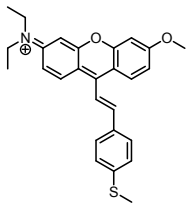	**130**	**654**	**72**	***This work***

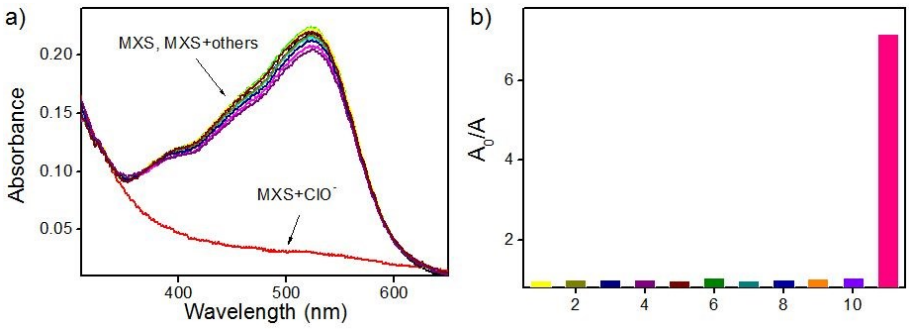

Fig. S2. Absorption responses of **MXS** (10 μM) in the presence of different relevant analytes (5 equiv.) in PBS (10 mM, pH = 7.4), 1: $^1O_2$, 2: H_2O_2, 3: blank, 4: NO, 5: NO_2^-, 6: NO_3^-, 7: O_2^-, 8: •OH, 9: $ONOO^-$, 10: TBHP, and 11: ClO^-.

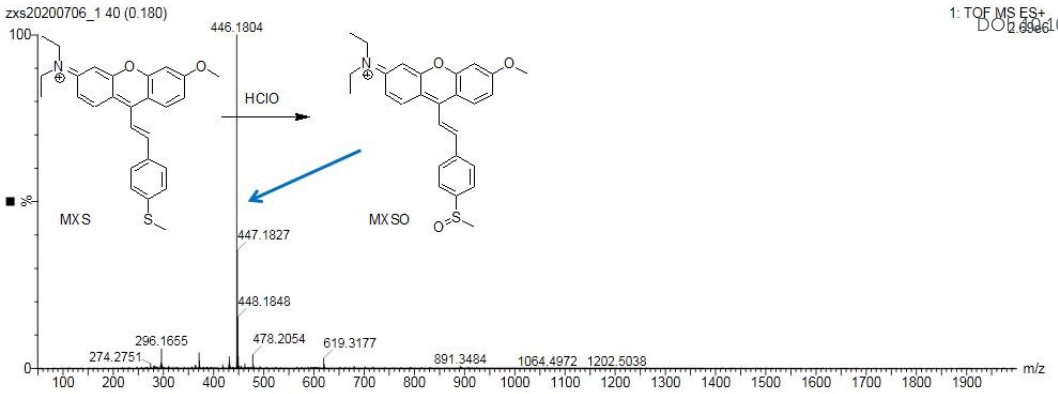

Fig. S3. HRMS spectra of **MXS** upon addition of OCl^-.

Table S3 Spectral data of **MXSO** in different solvents.

Solvents	λ_{abs} (nm)	λ_{em} (nm)	ε ($mol^{-1}cm^{-1}L$)	Φ[a]
DCM	533	570, 626	8900	0.082
EtOH	530	573, 628	6800	0.067
DMSO	536	631	6800	0.036
PBS	504	649	5700	0.018
MeCN	530	632	8300	0.031
DMF	533	578, 633	3300	0.053

[a] Relative fluorescence quantum yield estimated by using Nile Blue (Φ_B = 0.27 in ethanol)[1] as a fluorescence standard.

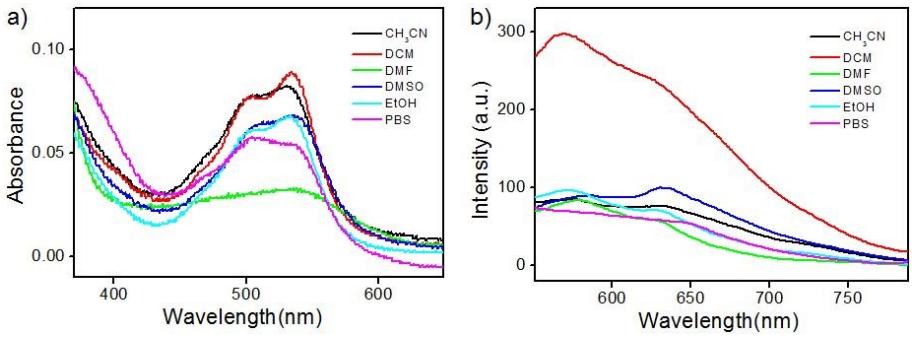

Fig. S4. Absorption and fluorescence spectra of **MXSO** in different solvents.

View Article Online
DOI: 10.1039/D0OB01563F

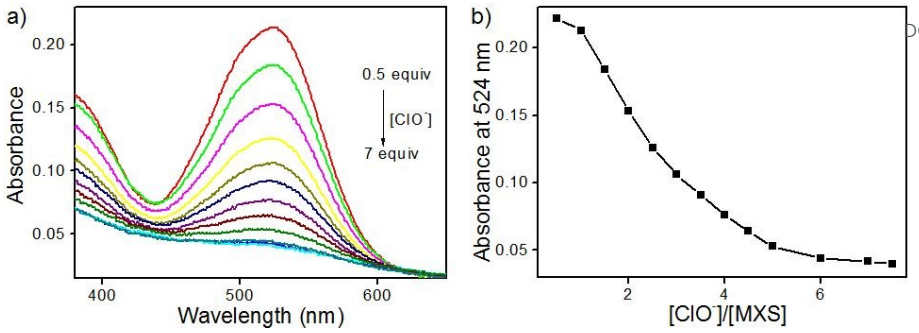

Fig. S5. (a) The absorption changes of **MXS** (10 μM) treated with increasing concentrations of OCl^- (0.5 – 7 equiv.) in PBS (10 mM, pH = 7.4). (b) The plot of the fluorescence intensities at 524 nm versus the equivalents of OCl^-.

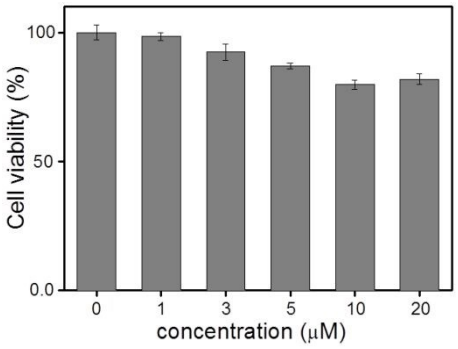

Fig. S6 MTT assay of **MXS**.

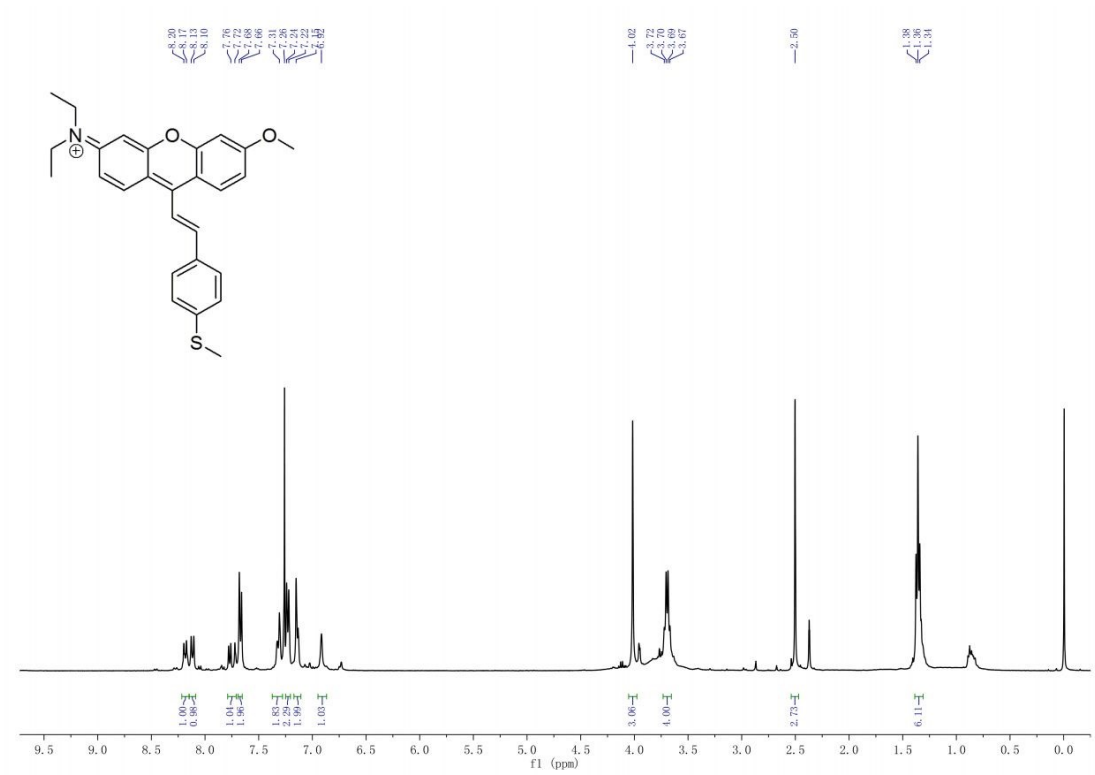

Fig. S7 ^{1}H NMR spectra of **MXS** in $CDCl_3$

View Article Online
DOI: 10.1039/D0OB01563F

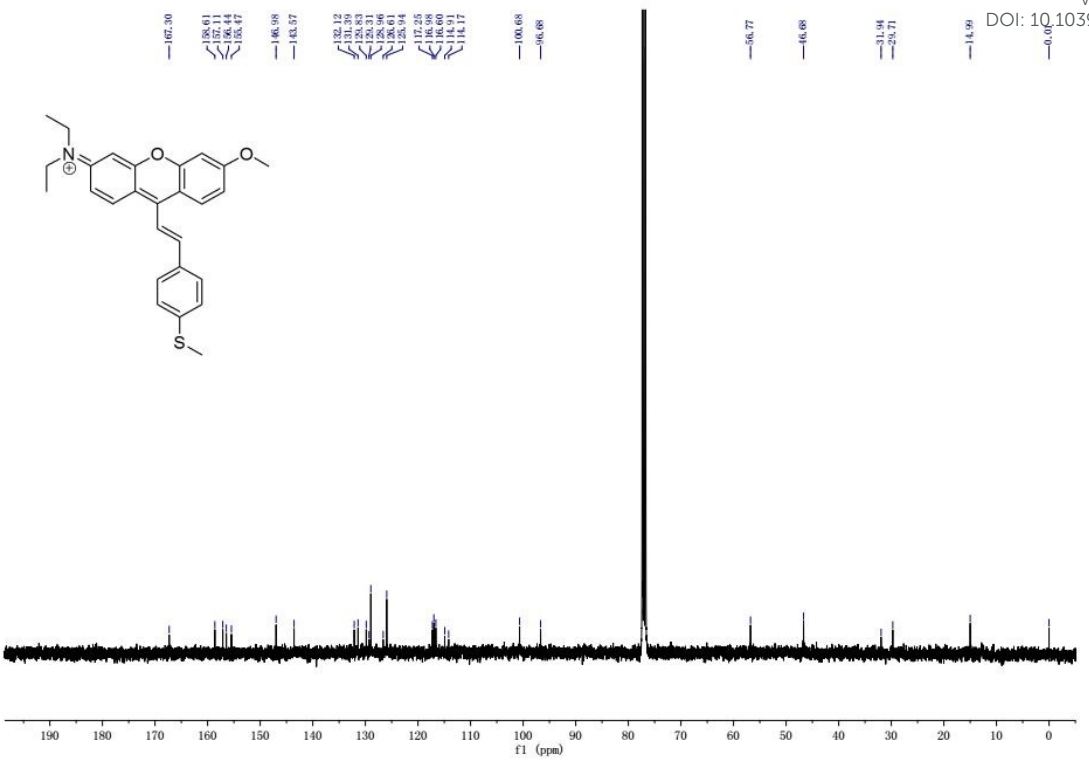

Fig. S8 ^{13}C NMR spectra of **MXS** in $CDCl_3$

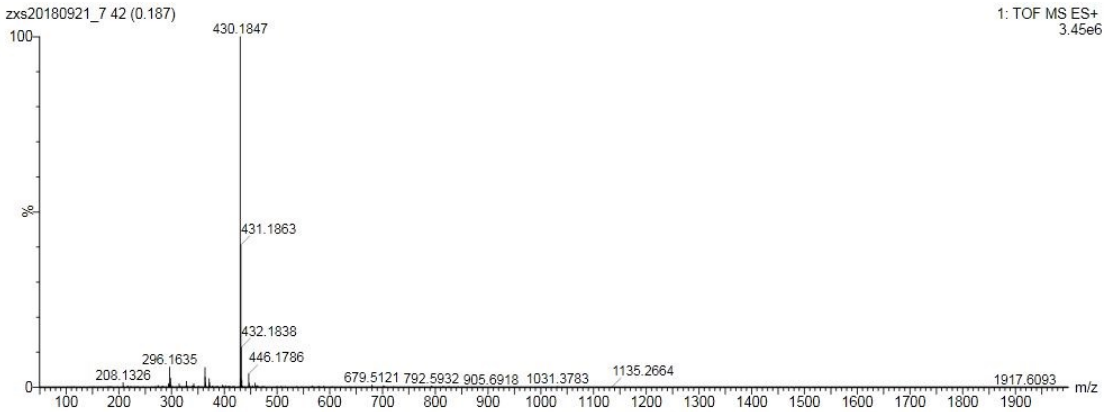

Fig. S9 HRMS spectra of **MXS**

View Article Online
DOI: 10.1039/D0OB01563F

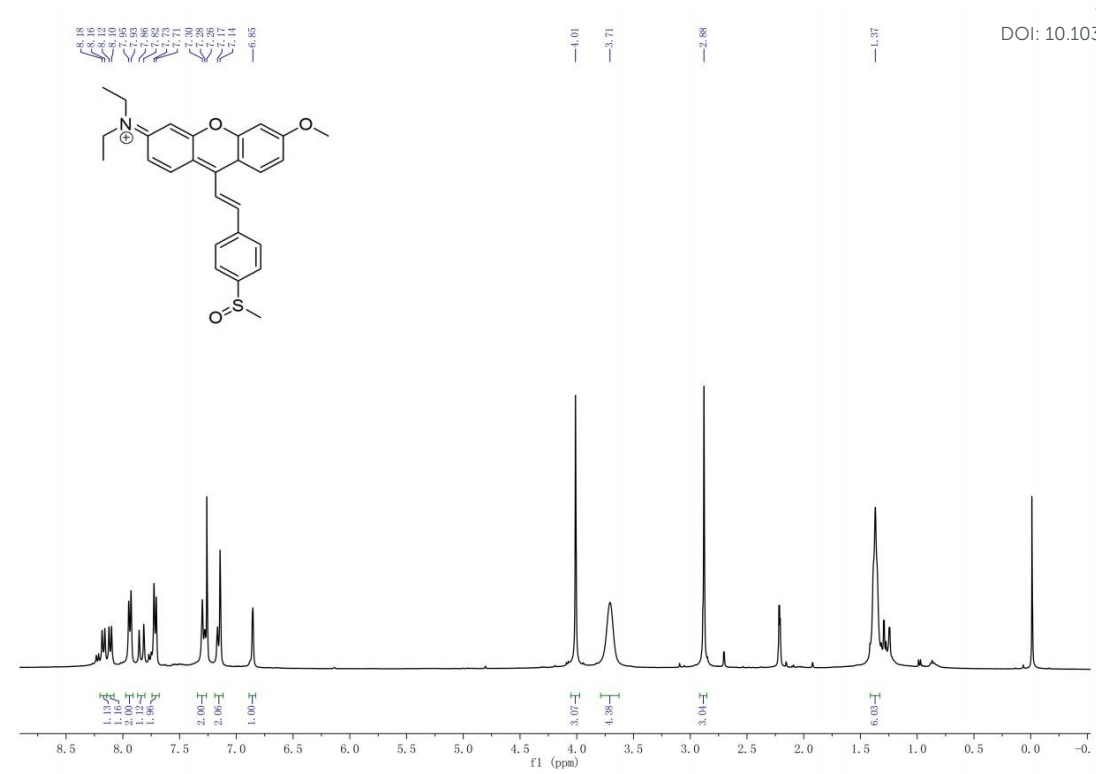

Fig. S10 ^{1}H NMR spectra of **MXSO** in $CDCl_3$ (400 MHz).

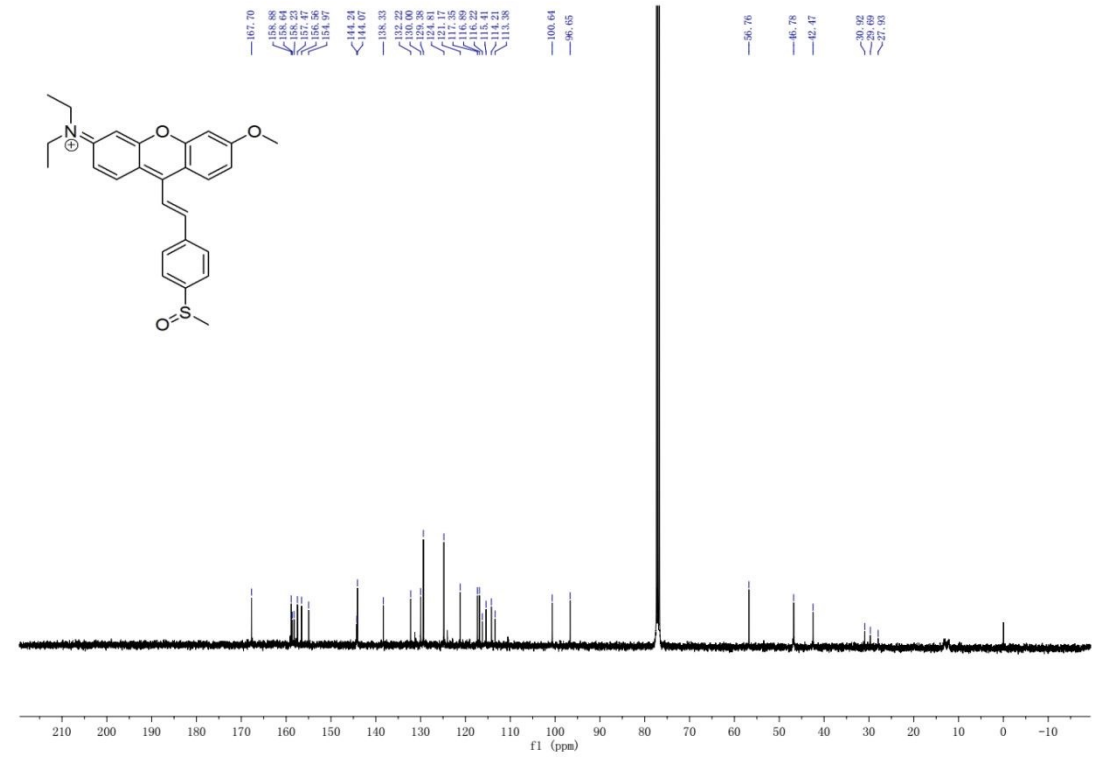

Fig. S11 ^{13}C NMR spectra of **MXSO** in $CDCl_3$ (100 MHz).

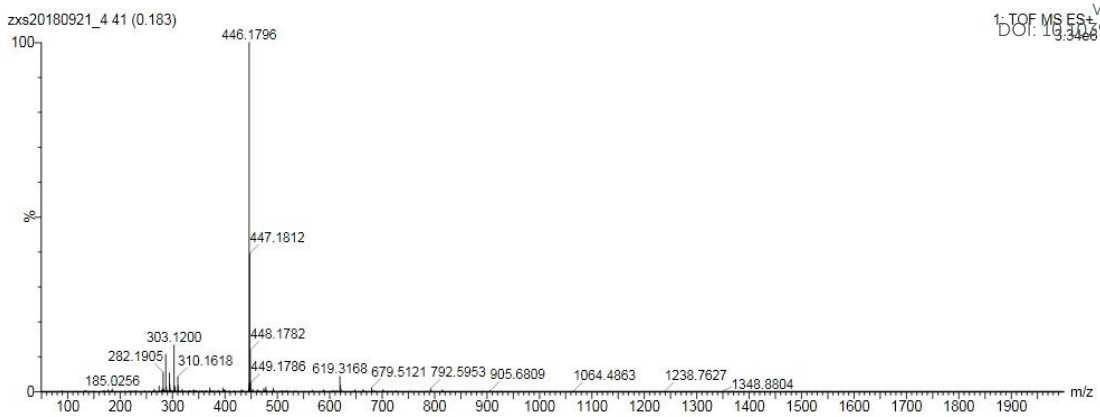

Fig. S12 HRMS spectra of **MXSO**.

References:

1. R. Sens, K. H. Drexhage, *J. Luminesc.*, 1981, **24**, 709.